Journal of Bionic Engineering
https://doi.org/10.1007/s42235-023-00453-8

Robust machine learning mapping of sEMG signals to future actuator commands in biomechatronic devices

Ali Nasr · Sydney Bell · Rachel L. Whittaker · Clark R. Dickerson · John McPhee

Received: 16 February 2023 / Revised: 27 October 2023 / Accepted: 8 November 2023 / Published online: 19 December 2023

Abstract A machine learning model for regression of interrupted surface electromyography (sEMG) signals to future control-oriented signals (e.g., robot's joint angle and assistive torque) of an active biomechatronic device for high-level myoelectric-based hierarchical control is proposed. A recurrent neural network (RNN) was trained using output data, initially obtained from offline optimization of the biomechatronic (human-robot) device and shifted by the prediction horizon. The input of the RNN consisted of interrupted sEMG signals (to mimic signal disconnections) and previous kinematic signals of the assistive system. The RNN with a 0.1-second prediction horizon could predict the control-oriented joint angle and assistive torque with 92% and 86.5% regression accuracy, respectively, for the test dataset. This proposed approach permits a fast, predictive, and direct estimation of control-oriented signals instead of an iterative process that optimizes assistive torque in the inverse dynamic simulation of a multibody human-robot system. Training with these interrupted input signals significantly improves the regression accuracy in the case of sEMG signal disconnection. This robust predictive control-oriented machine learning (RobustMuscleNET) model can support volitional high-level myoelectric-based control of biomechatronic devices, such as exoskeletons, prostheses, and assistive/resistive robots. Future work should study the application to prosthesis control as well as the repeatability of the high-level controller with electrode shift. The low-level hierarchical controller that manages the human-robot interaction, the assistance/resistance strategy, and the actuator coordination should also be studied.

A. Nasr
University of Waterloo, Waterloo, Ontario, Canada
E-mail: a.nasr@uwaterloo.ca

Keywords Myoelectric-based Control · Electromyography · Machine Learning · Multibody System Dynamics · Exoskeleton

1 Introduction

The state-of-the-art control of biomechatronic devices, such as robotic exoskeletons, prosthesis, and rehabilitation systems, employs a hierarchical design (high and low-level controllers [1–3]) for rehabilitation, power augmentation, and artificial replacements of body segments [4–7]. The high-level controller is in charge of interpreting the user's motion [7–11] or the wrench employed by the user (torque and force) [2, 8, 12]. The low-level controller considers the determined intended motion or wrench from the high-level controller and regulates the biomechatronic actuators according to the human-robot interaction model and assistive/resistive regulations [3, 8].

The high-level control system may use human motion prediction as one of the feedback signals [2, 9, 13, 14]. To predict human motion, the three main categories of signals used are kinematic (position, velocity, or acceleration) [15], kinetic (force or torque) [13, 14, 16], and bioelectric signals (cognitive human-robot interaction) [7–9, 11]. Bio-signals are one of the principal inputs of high-level controllers embedded within biomechatronic devices, rehabilitation robots, prostheses, and exoskeletons [1, 5, 8, 9]. Amongst bio-signals, surface electromyography (sEMG), the measurement of the electrical activity generated to produce muscle contraction, has demonstrated potential in illuminating human motion intention for controlling biomechatronic devices [1, 7, 8, 14, 17].

Using wearable myoelectric sensors for daily living activities has challenges and limitations discussed in the following paragraphs. One challenge with using myoelectric sensors is that signal disconnection or the wearable sensors losing contact from the skin is inevitable [18]. sEMG signals may have signal loss due to electrode disconnection, battery loss, muscle artifacts, or impractical for deep muscles [18, 19]. In these cases, the myoelectric-based control would likely fail. Thus, preparing a robust prediction model for signal disconnection is necessary.

The second challenge relates to the delay of mapping the sEMG signals to the outputs in the control algorithm. Specifically, recording delay, transmitting, digitizing, filtering raw signals, and employing complex equations or mapping via a multilayer neural network to the output signal is time-consuming [20–22]. Having a model that can predict future human intent can help in predictive control [11]. Theoretically, the electromechanical delay phenomenon is defined as the time delay between the onset of the sEMG and the onset of the human motion [23, 24]. In other words, since the muscle activation signals are generated before the production of torque at a joint, it is possible to use sEMG signals to predict motion intent [21, 25]. Thus, it is hypothetically possible to predict future motion from the current sEMG signal [22]. A solution to predict motion intention or future joint torque using sEMG signals is beneficial in myoelectric control.

The third challenge emerges from differences in the configuration of robotic joints compared with human joints and a requirement of extra conversion. For example, a shoulder exoskeleton may have one joint for the elevation angle, although a human shoulder joint may be defined by shoulder flexion/extension (SFE) and shoulder adduction/abduction (SAA) [4, 26, 27]. Therefore, transferring the human joint variables to robot joint variables is necessary and sometimes uses time-consuming iterative calculations [26, 27]. To satisfy the mentioned objective of the control-oriented model, we propose to have a model with outputs of the control-oriented variables (robot assistive torque or joint angle) instead of human variables (human joint torque or joint kinematics). The conversion should be done offline, and the resultant variables are the mapping target of a machine learning model.

Determining the optimal assistive wrench profile supplied by biomechatronic devices throughout human motion is an ongoing challenge [28]. Most researchers have used a time-consuming optimization method in offline simulation [29–31]. For example, Zhang et al. [32] introduced an iterative process that optimizes the assistive torque profile for one stride of walking in one hour of computation to minimizes human energy cost during walking. Additionally, the human-robot system has redundant actuation, and finding the optimum torque profile is complicated. Although fast online optimization methods have been suggested [28, 33, 34], they struggle to run in real-time with sufficient model fidelity. Thus, the control loop of active biomechatronic devices should preferentially use the offline optimized result of an iterative optimization process. Consequently, inefficient online optimization for assistive control loops is not necessary. Recently, the regression of sEMG signal to biomechanical signals (human joint angle, velocity, acceleration, and torque) has been studied using machine learning models [13, 35–38]. We used the proposed machine learning model in [8], specifically the recurrent neural network (RNN); this model's inputs and outputs were adjusted to mitigate the aforementioned challenges with sEMG signal loss and delay.

The myoelectric-based control should be fast in terms of computation costs and robust in terms of responsiveness to myography challenges [39]. The controller should predict the future state, define the assistive torque profile, and require no extra conversion of human to robot metrics. In this work, we propose a machine learning model with three features:

1. Robustness: The model is robust to sEMG signal disconnections and trained to anticipate signal loss, a common challenge in sEMG signal recording [19].
2. Predictive: The output of the proposed model is future or shifted signals, which are helpful in predictive control.
3. Control-oriented: The output signals are the robot's joint angle and joint assistive torque instead of human biomechanical signals, eliminating time-consuming iterative conversion [29–31].

In total, the proposed RNN model, robust predictive control-oriented machine learning (RobustMuscleNET) model, regresses the interrupted sEMG signals to the robot's future joint angle and assistive torque. Critically, the configuration of RNN should be optimized to meet the new input-output signals. In summary, this work's distinguishing characteristics are:

1. regression-based mapping for predicting the future motion of a biomechatronic device;
2. estimating the control-oriented torque without additional iterative optimization in the control loop;
3. using a data preparation algorithm for robust mapping of interrupted sEMG signals;
4. evaluating machine learning-driven control in human-in-the-loop (HITL) experiments; and
5. proposing a volitional myoelectric-based control of biomechatronic devices, such as exoskeletons, prostheses, and assistive / resistive robots.

The main novelties of this work are a robust mapping of interrupted sEMG signals and using future control-oriented signals instead of the current human biomechanical variables. Combining the mentioned solutions produces RobustMuscleNET model for myoelectric control of biomechatronic devices. To the best of our knowledge, using interrupted sEMG signals to train a machine learning model, along with the offline optimization of the required assistive torque profile as the output, has not been studied yet.

It is noteworthy that the assistive / resistive regulation and human-robot interaction model in the low-level hierarchical controller is out of the scope of this research. Although the electrode shift from one subject to another is evaluated using different subjects for machine learning estimation and testing, the electrode shift challenge of one specific subject is out of the scope of this research.

In this paper, firstly, the configuration of the machine learning model is described. Secondly, the initial data collection steps are explained. Thirdly, the novel data preparation for the robust predictive machine learning models is introduced. Finally, the results and evaluations of the model are discussed.

2 Recurrent neural network (RNN)

The machine learning model for estimating the control signal in this research is a RNN model [8]. Specifically, a nonlinear autoregressive with external input neural (NARX) network configuration was selected as the RNN model to map the sEMG and delayed kinematic signals to the predicted robot's elevation joint angle and assistive torque. The NARX network has a feedback connection and is generally used in time-series modeling. The primary equation of the NARX model is provided in Equation (1). A schematic of the RNN model with one hidden layer is demonstrated in Figure 1.

$$y(t) = f[\, y(t-1), y(t-2), \cdots, y(t-n_y), \\ u(t), u(t-1), \cdots, u(t-n_u)] \quad (1)$$

where

$y(t)$	current output signal
$u(t)$	current input signal
n_u	number of prior values of the input signal
n_y	number of prior values of the output signal

2.1 RNN configuration

The configuration of the RNN model plays an essential role in modeling performance and regression accuracy.

Table 1: The optimization variables of RNN configuration (90 different RNN configurations as a full combination of all variables).

Variable (Symbol)	Minimum	Maximum	Step
hidden layers (n_l)	1	2	1
nodes in each hidden layer (n_n)	10	50	10
input signal previous values (n_u)	1	5	2
output signal previous values (n_y)	1	5	2

This configuration should be tuned for the nature of inputs (sEMG and exoskeleton's kinematic signals) and outputs (control-oriented signals). The variables of the RNN configuration contain n_u, n_y, the number of layers (n_l), the number of nodes in each layer (n_n), and the activation functions. This research tested 90 different RNN configurations, assessed the estimation accuracy, and adopted the superior configuration. The minimum variables, maximum variables, and step changes are presented in Table 1. Since the output signals are normalized by the maximum signal value and are always between 0 and 1, we have employed a symmetric saturating linear transfer function for the output activation function (Figure 1).

2.2 Model training and evaluation

In this research, 17 participants' empirical data sets were used. Two different participants' data sets (11.7%) were used to validate and extract the general model. In addition, one participant's data set (5.9%) was used to test the estimation capability of the model. The number of samples was $561000 = 17 \times 60 \times 50 \times 11$, since the data used was recorded from 17 participants, in 60 seconds, re-sampled at 50 Hz, and interrupted 11 times. The Levenberg–Marquardt backpropagation algorithm was used to train the RNN model. The backpropagation algorithm calculates the Jacobian of the training performance regarding the bias and weight variables of the RNN network. The initial adaptive mu, mu decrease factor, mu increase factor, and maximum mu values were 0.001, 0.1, 10, and 1e10. The epoch was set to 1000, and the training time was limited to less than one hour. The training was terminated when the epoch or the time reached the maximum values. Although the network is not deep, the model was configured to be closed-loop instead of open-loop for the training purposes of time-series data, which requires ten times the amount of training time. Additionally, the data is multiplied by the number of signal disconnection possibilities. For example, for 1, 2, and 3 disconnections, the

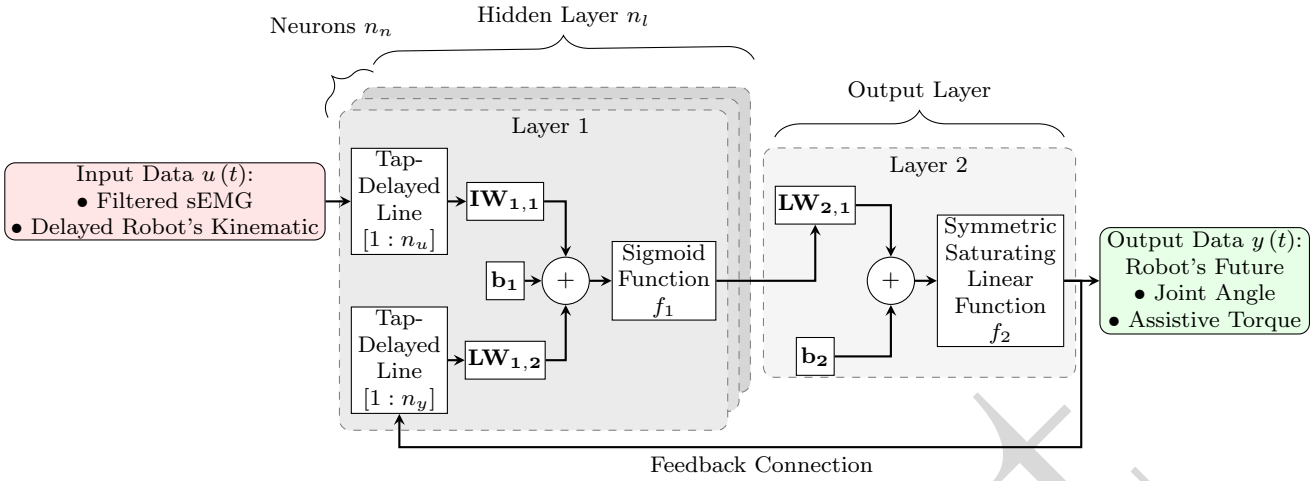

Fig. 1: A schematic of a RNN model with one hidden layer. $u(t)$ and $y(t)$ are the input and the output signals, respectively. n_u and n_y are the number of prior values of the input and output signal, respectively. IW, LW, and b are the input weight, layer weight, and bias of one neuron, respectively.

data volume is multiplied by 11, 110, and 990, respectively. We found the training time selection relevant to the computation capability of the PC to be reasonable. The training performance was assessed using the mean squared normalized error (MSE) function. The linear regression of targets relative to outputs (R) was used for reporting and evaluating the regression performance.

Using a subject that has not participated in the training and validation process for estimation evaluation purposes provided the opportunity for electrode shift evaluation, which is another challenge for daily prosthesis use [40–42]. Electrode placement, human body characteristics, muscle strength, and skin thickness differ from one participant to another. Generally, when using different participants for validation and testing in a machine learning model with a wide configuration network, the electrode shift is assessed between participants, and the full estimation accuracy is estimated via data of a random participant.

3 Data collection

- **Participants:** Nine female and eight male healthy right-handed individuals (23±4 years; 72.25±29.85 kg mass; 1.66 ± 0.16 m height) gave informed consent and performed proscribed object manipulation tasks. The experimental protocol was in accordance with the Declaration of Helsinki. The university office of research ethics approved the data collection study (ORE #: 21246).
- **Instrumentation:** 3D position data of bony landmarks of the torso, upper arm, and forearm segments were obtained using eight Vicon MX20+ cameras (Vicon Motion Systems, Oxford, U.K.) at a sample rate of 50 Hz [43]. The task targets and load positions also had reflective markers.
  Surface electromyography of the serratus anterior, deltoid (anterior, posterior, middle), supraspinatus, infraspinatus, trapezius (upper, middle, lower), latissimus dorsi, and pectoralis major muscles were measured using Noraxon Bipolar Surface Ag-AgCl electrodes with a fixed 2 cm inter-electrode distance (Noraxon Inc, Arizona, USA) and a Noraxon T2000 telemetered system, TeleMyo, (Noraxon Inc, Arizona, USA). The skin overlying these muscles (a total of 11 sites) was shaved and wiped with an alcohol swab prior to placing the electrodes. Electrode placement followed previous work and was confirmed through palpation [44, 45]. A reference electrode was placed over the clavicle. Subsequently, the raw signals were amplified (common-mode rejection ratio ≥ 100 dB at 60 Hz, input impedance 100 MΩ), sampled at a rate of 1500 Hz, and digitized (16-bit A/D card, maximum ±10 V).
- **Task protocol:** The individuals were asked to lift a weighted bottle from the lower target, place it on the upper target, and contrariwise 15 times in 60 seconds following the beat of a metronome [43, 46]. Participants were requested to rest/pause for around 2 seconds at the targets. The pose of the participants is shown in Figure 2(a). The weighted object was a 14.9 ± 6.6 N weight, scaled to the participant's shoulder elevation strength [46].
  During data collection, participants had no interaction with an assistive biomechatronic device (Figure 2(a)) since the device impacts human behaviour,

(a) Measurement [8, 46]

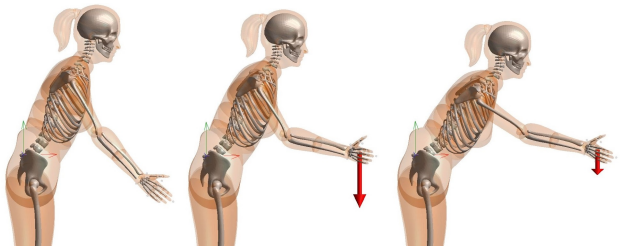

(b) MapleSim human musculoskeletal model [50]

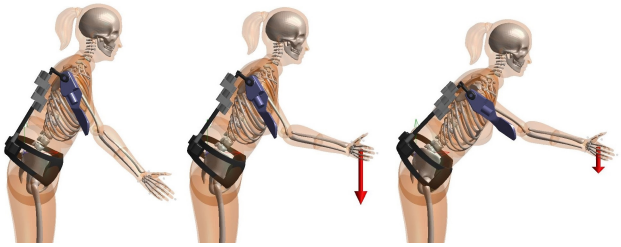

(c) MapleSim human-exoskeleton biomechatronic model [51]

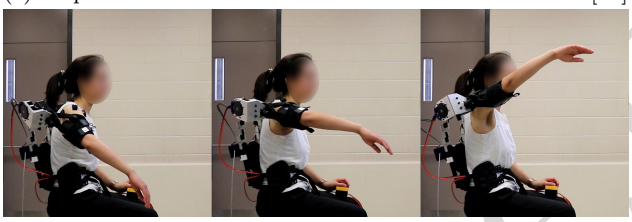

(d) Human-exoskeleton free movement experiment

(e) Human-exoskeleton lifting experiment

Fig. 2: A depiction of the data collection process where participants delivered and returned a weighted object between target locations (a). A sample of the human musculoskeletal (b) and human-exoskeleton (c) MapleSim models. A sample of the human-exoskeleton experiment for free movement (d) and weight lifting (e).

decreases measurement accuracy, and the human adapts to the assistive wrench [47–49]. However, the exoskeleton dynamic model (Figure 2(c)) can be added to the human model (Figure 2(b)) via simulation. The human-exoskeleton model is explained in detail in section 4.1.

4 Data preparation

The data preparation information regarding the objective of RobustMuscleNET model has been presented in the following section. The machine learning model's target output is the future exoskeleton elevation joint angle and the assistive torque, which would be used in lower-level controllers of exoskeletons. The inputs of the machine learning model are the interrupted sEMG signals and the delayed kinematic signals of the robot.

One of the objectives of the model for controlling biomechatronic devices is to provide a fast mapping. From a control viewpoint, it is better to have minimal kinematic and dynamic computation in real-time controlling. Thus, providing a control-oriented model instead of a human-oriented model plays a vital role in decreasing the computation cost. These extra kinematic and dynamic computations are due to the kinematic structure, joints, links, and constraints of biomechatronic devices, leading to biomechatronic joints that are not co-axial with human joint axes. Consequently, it is impossible to lump the assistive / resistive robot link inertial properties with that of the human segmental body and therefore intractable to use ordinary differential equations (ODEs). Since the human-mechatronic devices may have closed kinematic chains in the multibody model, we must solve differential-algebraic equations (DAEs), which requires time-consuming optimization loops. Thus, conversion from human joint variables to robot control command is not required in assistive robots' real-time high-level control. However, the conversion should occur a priori via an offline simulation to prepare the control-oriented model's training data. The offline simulation can be obtained by optimizing the robot's assistive torque through the multibody dynamic model simulation.

4.1 Output 1: Future assistive torque

The multibody system consists of six sub-systems:

– The central nervous system (CNS) (comprised of the brain and spinal cord that controls, coordinates, and manages the musculoskeletal (MSK) system) was modelled using nonlinear model predictive control (NMPC) [4, 48]. NMPC combines features of motion prediction and error correction using an internal model (IM) to estimate measures such as effort and feasibility. The CNS controller optimizes a cost function (Equation (2)), subject to biomechanical limitations (Equation (3)). More information on the weights and the prediction horizon is available in [48];

– The muscular system was created using muscle torque generators (MTGs) that include four torque sub-functions as shown in Equation (4) [52]. The sub-functions are: (I) the passive torque (τ_p), (II) peak joint strength (τ_0), (III) active-torque-angle scaling (τ_θ), and (IV) active-torque-angular-velocity scaling (τ_ω). These sub-functions are considered separately for positive and negative directions and are scaled by sex, age, body mass, body height, dominant side, and physical activity;
– The skeletal system was created using body segment inertial parameters (BSIPs) and was developed to have 20 degrees of freedom (DoFs), which were defined according to International Society of Biomechanics (ISB) standards [53];
– The wearable/biomechatronic structure was designed such that any device could be considered. Here, we selected the EVO (Ekso Bionics Holdings Inc, California, USA) upper limb exoskeleton model as our biomechatronic system. The EVO's model was experimentally verified in [4]. The skeletal system and the exoskeleton's frame (Figure 2(c)) form a closed kinematic chain in the multibody model (which consists of position (Equation (6)), velocity (Equation (7)), and acceleration (Equation (8)) level constraints);
– The assistive torque optimization system was designed to reduce muscle tension and human joint torque. An optimization loop was defined to solve for the exoskeleton's assistive elevation torque by minimizing a cost function (Equation (9)) [54];
– The actuator or the motor's torque-producing ability was expressed using Equation (10), which is how the torque production is typically expressed without considering the motor-armature inductance.

Simulation of the aforementioned multibody model has the following four steps. The resultant simulation computes assistive torque (T_d) and the robot kinematic data (ϕ_t, $\dot{\phi}_t$, and $\ddot{\phi}_t$).

1. The human joint angle measurements ($\boldsymbol{\theta}_d$) were filtered with a 10 Hz low-pass filter (minimizing high-frequency noise in the measurements). The human joint velocities ($\boldsymbol{\omega}_d$) were obtained using numeric derivatives and a 20 Hz low-pass filter;
2. These processed kinematic data were used as the reference trajectory for the cost function in Equation (2) and as the CNS-NMPC coordinates for the human body to determine the activation signal ($\boldsymbol{a}$) with respect to Equation (3). The activation signal was fed to the MTG model in Equation (4) to calculate the human joint torque ($\boldsymbol{\tau}_h$);
3. The cost function used for assistive torque optimization (Equation (9)) was applied to minimize the human joint torque (τ_h), especially shoulder joint, by providing exoskeleton assistive torque (T_d). Then, the assistive torque was used in Equation (10) to consider the motor dynamics.
4. The human ($\boldsymbol{\tau}_h$) and exoskeleton (T) torques were used as inputs for forward dynamic simulation of the model in Equation (5). Equation (5) is solved with respect to the position, velocity, and acceleration constraints in Equations (6-8), which form a DAE and require a high computation cost compared to an ODE.

$$J_{CNS} = \int_t^{t+t_p} [\, \mathbf{W}_1^T \left(\boldsymbol{\theta} - \boldsymbol{\theta}_d\right)^2 + \mathbf{W}_2^T \left(\boldsymbol{\omega} - \boldsymbol{\omega}_d\right)^2 + \mathbf{W}_3^T \left(\boldsymbol{a}\right)^2 + \mathbf{W}_4^T \left(\dot{\boldsymbol{a}}\right)^2] dt \tag{2}$$

$$\begin{aligned} \boldsymbol{\theta}_{min}\left(\beta\right) \le \boldsymbol{\theta} \le \boldsymbol{\theta}_{max}\left(\beta\right) \\ \boldsymbol{\omega}_{min}\left(\beta\right) \le \boldsymbol{\omega} \le \boldsymbol{\omega}_{max}\left(\beta\right) \\ -1 \le \boldsymbol{a} \le 1 \\ \dot{\boldsymbol{a}}_{min} \le \dot{\boldsymbol{a}} \le \dot{\boldsymbol{a}}_{max} \end{aligned} \tag{3}$$

$$\begin{aligned} \boldsymbol{\tau_h} = \quad & \boldsymbol{a}^+ \boldsymbol{\tau}_\omega^+ \left(\boldsymbol{\omega}, \beta\right) \boldsymbol{\tau}_\theta^+ \left(\boldsymbol{\theta}, \beta\right) \boldsymbol{\tau}_0^+ \left(\beta\right) + \\ & \boldsymbol{a}^- \boldsymbol{\tau}_\omega^- \left(\boldsymbol{\omega}, \beta\right) \boldsymbol{\tau}_\theta^- \left(\boldsymbol{\theta}, \beta\right) \boldsymbol{\tau}_0^- \left(\beta\right) + \boldsymbol{\tau}_p \left(\boldsymbol{\theta}, \boldsymbol{\omega}, \beta\right) \end{aligned} \tag{4}$$

$$\mathbf{M}\dot{\mathbf{p}} + \mathbf{C}^T \boldsymbol{\lambda} = \mathbf{F} + \mathbf{Q} \tag{5}$$

$$\Phi(\mathbf{q}, t) = 0 \tag{6}$$

$$\Psi(\mathbf{p}, \mathbf{q}, t) = 0 \tag{7}$$

$$\chi(\dot{\mathbf{p}}, \mathbf{p}, \mathbf{q}, t) = 0 \tag{8}$$

$$J_A = \int_0^{t_f} \left[\boldsymbol{w}\boldsymbol{\tau}_{\boldsymbol{h}}^2\right] dt \tag{9}$$

$$T = NT_d - \left(N^2 I_m \ddot{\varphi} + N^2 b_m \dot{\varphi}\right) \tag{10}$$

where

J_{CNS}	CNS-NMPC cost function
t_p	prediction horizon
$\mathbf{W}$	CNS cost function weights
$\boldsymbol{\theta}$	human joint angles
$\boldsymbol{\omega}$	human joint instantaneous angular velocities
$\boldsymbol{a}$	activation signal
$\dot{\boldsymbol{a}}$	rate of activation signal
$_d$	desired value or trajectory
$_{min}$	minimum variable
$_{max}$	maximum variable
β	subject adjustment variables: sex, age, body mass, height, dominant side, and physical activity
$\boldsymbol{\tau}_h$	human joint torque
$^+$	positive direction of joint
$^-$	negative direction of the joint
$\boldsymbol{\tau}_\omega$	the active-torque-angular-speed-scaling function

$\boldsymbol{\tau}_\theta$	the active-torque-position-scaling function
$\boldsymbol{\tau}_0$	the peak isometric joint strength producing capability
$\boldsymbol{\tau}_p$	the passive torque function due to viscous damping and nonlinear stiffness
n	number of joints
m	number of constraint reactions
$\mathbf{M}$	$n \times n$ mass matrix, a combination of the human and the exoskeleton models
$\mathbf{C}$	$m \times n$ constraint Jacobian (maps reaction forces/torques to generalized forces)
$\boldsymbol{\lambda}$	$m \times 1$ reaction forces and torques in the cotree joints that enforce the kinematic constraint of human-exoskeleton connection
$\mathbf{F}$	$n \times 1$ right-hand side of dynamic equations
$\mathbf{Q}$	$n \times 1$ generalized force vector containing the applied wrench (torque/force) at the joints, which consists of the human joint torque ($\boldsymbol{\tau}_h$) and the robot joint torque (T)
$\boldsymbol{\Phi}$	$m \times 1$ position-level kinematic constraint equations
$\boldsymbol{\Psi}$	$m \times 1$ velocity-level kinematic constraint equations; if the generalized speeds are equal to the coordinate derivatives, then $\Psi = \dot{\Phi}$
$\mathbf{q}$	n generalized coordinates of the multibody system, which consist of the human joint angles ($\boldsymbol{\theta}$) and the robot joint states ($\boldsymbol{\varphi}$)
$\mathbf{p}$	n generalized speeds of the multibody system, which consists of the human joint angular velocities ($\boldsymbol{\omega}$) and the derivative of robot joint states ($\dot{\boldsymbol{\varphi}}$)
J_A	assistive torque optimization cost function
t_f	final simulation time
$\boldsymbol{w}$	the cost function weights
T	the net motor output torque
N	the motor's gear ratio
T_d	the assistive torque applied to the rotor
I_m	the motor rotor inertias
b_m	the rotator viscous friction coefficients

4.2 Output 2: Future kinematic output signal

The electromechanical negative delay phenomenon [23] can compensate for the control system computation or actuation delay. We parameterized this phenomenon to predict the joint angle or motion intention using sEMG signals and a machine learning method. The predictive output signal can be obtained through two possible scenarios: (A) the future joint angle in the $t + \Delta t$ time or (B) the future joint acceleration using the Euler series. Both possible outputs are defined in the following paragraph.

For the current sEMG set in the time of t, the future joint angle $\phi_t + \Delta t$ in the time of $t + \Delta t$ was calculated by straightforward 1-D data extrapolation.

Similarly, since human motion (acceleration) is actuated by muscle contractions measured by the sEMG technique, the reference joint or task space acceleration can also be calculated from sEMG. The predicted acceleration $\ddot{\phi}'_h$ can be calculated by the Euler series for $t + \Delta t$ time in Equation (11) by using the current joint angle ϕ_t and joint velocity $\dot{\phi}_t$.

$$\phi_{t+\Delta t} \approx \phi_t + \dot{\phi}_t \Delta t + \frac{1}{2!}\ddot{\phi}'_h \Delta t^2 \tag{11}$$

The prediction horizon Δt plays an essential role in the accuracy of motion prediction. Therefore, we studied different values for the prediction horizon along with the possibility of the future joint angle $\phi_{t+\Delta t}$ or the predicted acceleration $\ddot{\phi}'_h$ as an output of the RobustMuscleNET model.

The assistive torque was shifted with $t + \Delta t$ as the prediction horizon to obtain the future assistive torque $\tau_t + \Delta t$.

4.3 Input 1: sEMG signal

– **sEMG filtering:** To prepare sEMG signals, raw signals were filtered in the following six steps (Figure 3):

Step #1 Band-pass filter with a normalized cut-off frequency of $20 - 500$ Hz to reduce the movement artifacts [55] and to remove the minor power spectral density [56] (Figure 3(c));

Step #2 Band-stop filter with a $55 - 65$ Hz normalized cut-off frequency (to reduce the 60 Hz impact from the measurement system) (Figure 3(e));

Step #3 Rectification of the signal value with the absolute function since muscles produce positive tension by activation [57] (Figure 3(g));

Step #4 A low-pass filter with a normalized cut-off frequency of 7 Hz to ignore extra frequency information outside the maximum human motion frequency [58, 59] (Figure 3(i));

Step #5 Normalization to the trial maximum signal amplitude for each participant. Additional filtering and analysis were unnecessary for a machine learning model for mapping signals (not a mathematical muscle model) [59] (Figure 3(k)).

Step #6 Sample rate reduction to 50 Hz, thus decreasing the computational cost of the model.

– **Interrupted sEMG signal:** As mentioned, one challenge with using myoelectric sensors is that signal disconnection or the wearable sensors losing contact

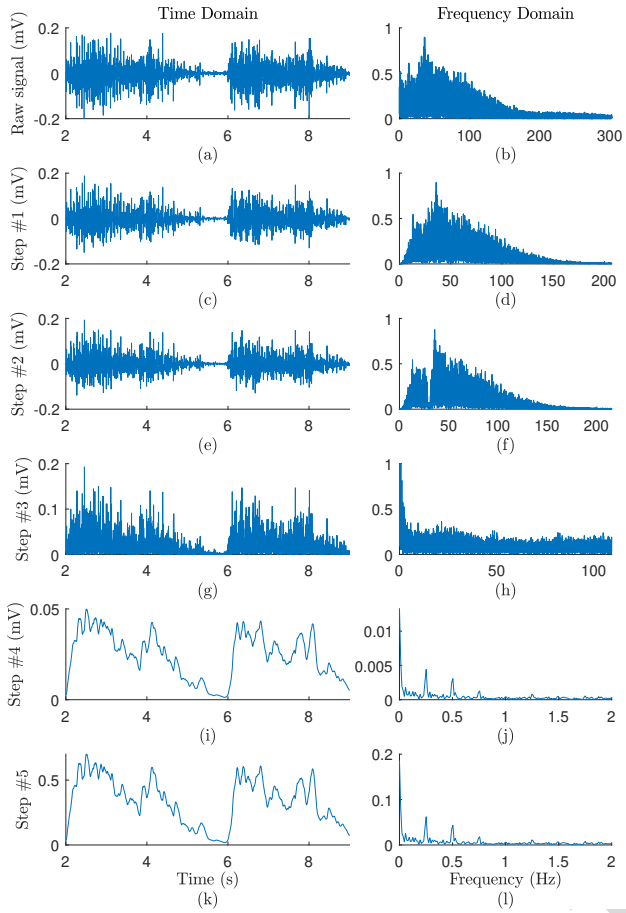

Fig. 3: Samples of the time and frequency domains of the raw and filtered sEMG signals.

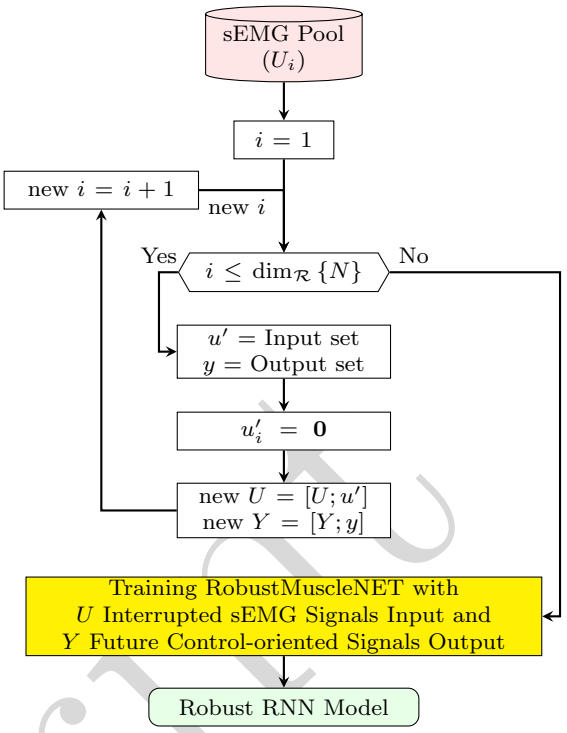

Fig. 4: Schematic of interrupting sEMG input signal algorithm.

from the skin is inevitable [18]. sEMG signals may have signal loss due to electrode disconnection, muscle artifacts, or the impracticality of measuring deep muscles [18, 19]. In these cases, the myoelectric-based control would likely fail. Thus, preparing a robust prediction model for signal disconnection is necessary. The intention for producing interrupted sEMG signals is to simulate this sEMG signal disconnection. Although in some situations, the signals' amplitude may only be reduced, we have considered the worst-case condition, which is complete disconnection. In this section, each input sEMG signal disconnects, and the output signals are intact. The volume of data samples is equal to the volume of the recorded data multiplied by the number of disconnections.

The dataset for training the robust model was produced according to the algorithm in Figure 4 and using the following steps:

i Initially set $i = 1$.

ii For the new input signal, multiply the input channel index i by zero.

iii If $i \leq N$ is satisfied, the index will be changed ($new\ i = i + 1$), and step (ii) will be repeated; if not, go to step (iv).

iv Train RobustMuscleNET model using the interrupted input signals and intact output signals.

Repeating steps (ii-iii) is similar to finding all combinations of N sEMG numbers, taking $N - 1$, and setting one signal at a time to a zero value (mimicking a disconnected signal). The zero value persist for each signal for whole trial and consequently the volume of training data increases by the number of sEMG channels. Multiplying more channels (e.g., the index i and j) by zero and applying the same strategy of assuming more sensors are disconnected is possible. After completing the described strategy, we have all common conditions which would likely happen to the input signals. As the RobustMuscleNET model was trained with this dataset, theoretically, it can estimate the output signals using less than N input signals.

4.4 Input 2: Delayed kinematic signal

The muscle model depends on the sEMG signals as well as kinematic signals. Thus, one of the muscle-based control model inputs was kinematic signals, including joint angle, velocity, and acceleration. The joint angle can be measured through rotary encoders or a rotary potentiometer, although the signal may have an electrical delay due to the connection speed and the sampling rate. Commonly, a low-pass filter with a computation delay of 0.025 seconds is used for filtering joint angle noises. The joint velocity and acceleration are estimable via the first and second derivatives using the current joint angle values, which have computation delays. Thus, we selected 0.025 seconds for the electrical delay modeling, and 0.025, 0.05, and 0.075 seconds for the computation delay of the joint angle, velocity, and acceleration signal. In total, the joint angle, velocity, and acceleration had delays of 0.05 seconds (0.025 electrical + 0.025 computation delay), 0.075 seconds (0.025 electrical + 0.05 computation delay), and 0.1 seconds (0.025 electrical +0.075 computation delay), respectively.

5 Experimental evaluation framework

- **Participants:** 21 healthy participants (12 males and 9 females; 25 ± 3.3 years; 66 ± 13.0 kg mass; 1.75 ± 0.09 m height; 2.5 ± 1.9 workout session per week; 15 right-handed and 5 left-handed) gave informed consent and performed the pick-and-place task. The custom exoskeleton was inspected by the safety office and the test protocol was given ethics clearance by the Research Ethics Board of the University of Waterloo (REB: #43980).
- **Instruments:** The Delsys Trigno wireless sEMG system (Delsys Inc, Natick, MA, USA) was used to measure the participants' muscle activity. The EVO (Ekso Bionics Holdings Inc, California, USA) upper limb exoskeleton structure was used as the biomechatronic system interacting with the human. An AK80-9 KV100 brushless direct current (BLDC) motor (Cubemars, Jiangxi Xintuo Enterprise Co., China) was augmented to fit the exoskeleton structure. The built-in motor driver communicated with the controllers through a controller area network (CAN-bus) and was calibrated through serial communication. An Arduino Uno and a CAN-bus Shield V2.0 (Seeed Technology Inc., Shenzhen, China) were used for communication between MATLAB and the motor. The mid-level controller from [48] was used to strengthen the RobustMuscleNET model's output and command the low-level controller of the motor's field-oriented control (FOC) unit.
- **Task:** Participants were allowed to move freely (Figure 2(d)) and lift a 5 pound kettlebell (Figure 2(e)) with their right arm while wearing the shoulder exoskeleton.

6 Results and discussion

The optimized configuration of the model and model performance evaluation are presented in the following paragraph. A personal computer with an Intel® Core™ i7-3370 CPU @ 3.40 GHz processor and 16.0 GB memory was used to prepare the data and train the machine learning model.

6.1 Control-oriented output

Using the control-oriented signals (the exoskeleton's joint angle and assistive torque) as the output of the RobustMuscleNET model decreased the calculation cost compared to using human biomechanical variable outputs (Figure 5). The conversion of the human biomechanical variables to the robot's kinematic and kinetic variables alternatively would require iterative time-consuming variables calculation (the algorithm shown in Figure 5(b)) with 0.1 s per frame of data for an assistive torque. This time-consuming iterative calculation is helpful for offline design [26]. However, this calculation cost is removed here since the model's output is the future exoskeleton's assistive torque and joint angle.

6.2 RobustMuscleNET model optimization

The RobustMuscleNET model was trained, validated, and tested with the 90 different configurations (section 2.1). Firstly, the top regression accuracy was obtained when the number of hidden layers (n_l) was 1. While having more hidden layers is possible, the training was limited to one hour, and the mapping slowed and required more memory as the number of hidden layers increased. Secondly, the optimal number of nodes in each layer (n_n) was approximately 30. With inadequate or spare nodes in each layer, the regression accuracy reduced or required more time for training, respectively. Thirdly, the number of input signal former values (n_u) was 3, which indicates that the history of biomechanical signals is essential for mapping. Finally, the number of the output signal former values (n_y) was required to be 3 for the optimum configuration. With more of the output signal's former values, the output becomes smoother. This result is quite similar to the configuration of the RNN model proposed as a machine learning muscle model [8].

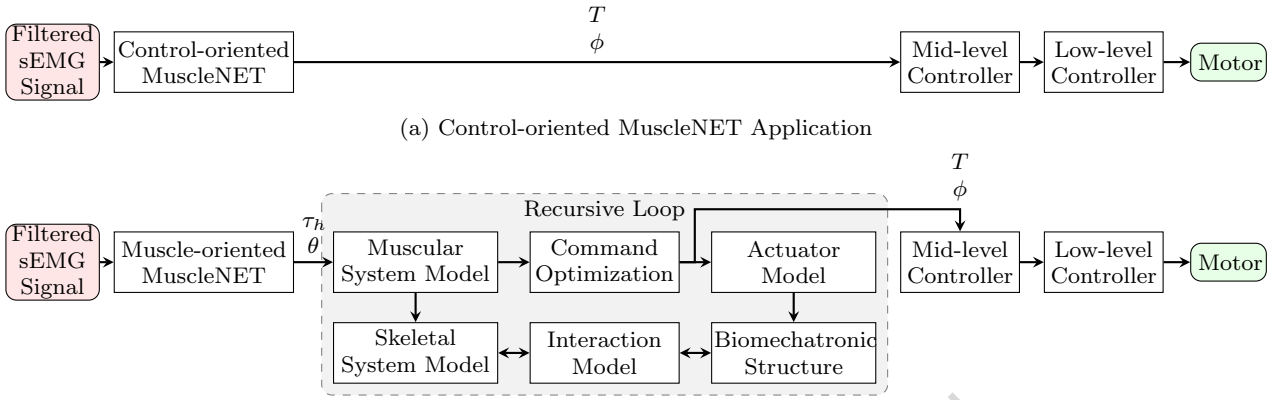

(a) Control-oriented MuscleNET Application

(b) Muscle-oriented MuscleNET Application

Fig. 5: Comparison of the control-oriented (a) and muscle-oriented (b) MuscleNET application for controlling biomechatronic systems while interacting with a human body. ϕ, θ, T, and τ_h are the robot joint angle, human joint angle, robot joint torque, and human joint torque, respectively.

6.3 Prediction horizon

The accuracy of the predictive model was assessed for two methods: angle prediction and acceleration prediction. The angle prediction $\phi_t + \Delta t$ used a time-shifted joint angle, and the acceleration prediction $\ddot{\phi}'_h$ used Equation (11). The shift, the positive delay range, or the prediction horizon was assessed between 0 and 0.5 seconc (Figure 6).

For the angle prediction in Figure 6, the regression accuracy dropped under 92% for a prediction horizon of more than 0.1 seconds. Thus, we recommend a prediction horizon of less than 0.1 seconds for the joint angle. This result approximates the electromechanical delay phenomenon [23]. For the acceleration prediction in Figure 6, the accuracy of the acceleration estimation was insufficient. Besides that, Equation (11) requires an accurate joint angle and velocity to predict the future joint angle. Thus, we do not propose to use Equation (11) for the joint prediction. If the biomechatronic device's current joint angle and velocity were measured with the highest accuracy and the estimation criteria were less than 92% regression accuracy for the validation and test datasets, Equation (11) could be used successfully.

The joint angle prediction was successful and had adequate accuracy (more than 90%) for less than 0.1 seconds (Figure 6). The amount is similar to the electromechanical delay phenomenon, defined as the time delay between the onset of the sEMG and the onset of the human motion [23]. Using this positive delay, the machine learning model could successfully predict the output signals for the next 0.1 seconds. The amount of electromechanical delay or prediction horizon may differ depending on individual body characteristics [24] and different tasks and can be evaluated using the same method.

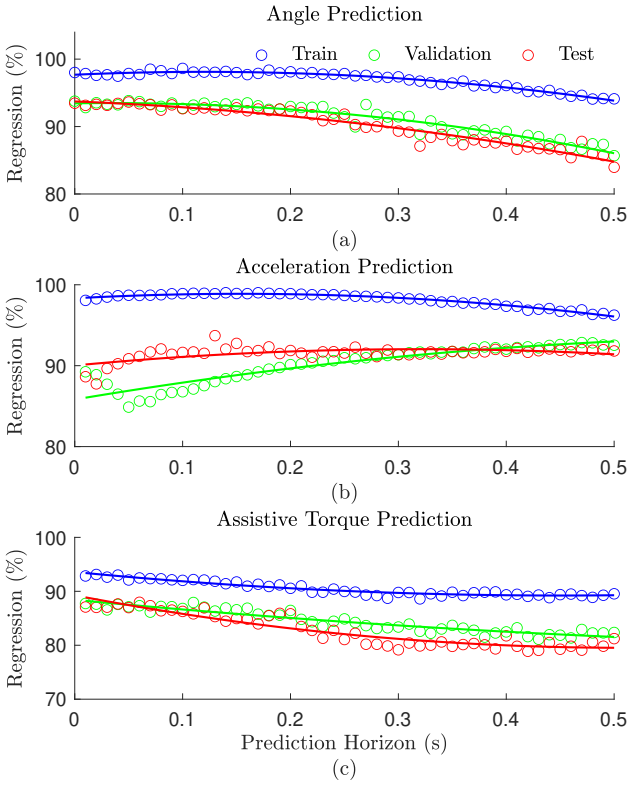

Fig. 6: The regression accuracy of the training, validation, and test data set for angle prediction and acceleration prediction.

For the assistive torque prediction in Figure 6, the regression accuracy dropped under 86.5% for a predic-

tion horizon of more than 0.1 seconds. This assistive torque prediction can be used in high-level predictive control of assistive devices. Using the future signals as the output of machine learning allows for real-time volitional high-level control of the biomechatronic system, and having the future intent provides the mechatronic device with the opportunity to be ready [7]. For example, the actuation system can run to serve in advance whenever the mapping system indicates a high amount of assistive torque for future steps.

6.4 Robust model evaluation

The estimation ability of normal and RobustMuscleNET models were also evaluated using interrupted signals (Figure 7). The input into the models was the interrupted sEMG and kinematic signals. For the evaluation, eleven sEMG signals were disconnected one by one. Two normal and RobustMuscleNET models were trained using different input signals and the same target signals. Specifically, the normal RNN model was trained with the ideal input signals without any disconnection. Subsequently, the RobustMuscleNET model was trained using the interrupted input signals.

The normal model had more error and sometimes misestimated the target signals (Figure 7), especially for the normalized assistive torque (regression of 71%). The RobustMuscleNET model handled the disconnection of input signals and estimated the output signals with regression accuracy of 92.3%. The higher regression accuracy of the RobustMuscleNET model indicates that the robust model is more suitable for practical application.

The normal and robust model with interrupted sEMG signal were also compared (Figure 8). All test participants' data was used to assess the estimation proficiency of the normal and robust model in the presence of sEMG disconnection. The robust model had $5-15\%$ more regression accuracy than the normal model when there is an interruption. This robust model thus addressed the issue of sEMG signal disconnection [18, 19]. An example of the estimation ability of normal and RobustMuscleNET models for a random participant is displayed (Figure 9).

The sEMG signal disconnections in section 4.3 are extended from 1 to 10 disconnections (for 11 sEMG channels in total), and the robust model was trained and compared to the normal model performance in the top part of Figure 8. The regression of the robust model with more disconnections generally decreases, but still is greater than the normal model. The regression accuracy for both robust and normal models drops below 50% for eight signal disconnections. This means that at least 4 sEMG signals should maintain connected for the shoulder exoskeleton device for more than 50% regression accuracy. The shoulder exoskeleton assists the 3-DoFs shoulder joint and requires 4 sEMG signals from at least 4 muscles to control the joint. This result of a minimum of 4 signals for a 3-DoFs joint is similar to what is seen in muscle synergies [60].

In the bottom part of Figure 8, the signals' impact was evaluated using sequential backward signal analysis. Each signal was deleted from the signal bank in the analysis, and the machine learning model was trained. Then, the deleted signal with the maximum regression was reported as the non-important signal. For example, the maximum regression was achieved with the lower trapezius (LTRA) deletion from the 11 signals database for the first analysis loop. The second analysis achieved the maximum regression with the LTRA and upper trapezius (UTRA) ignoration from the 11 signals database. In total, the order of least to most essential signals is: 11. LTRA, 10. UTRA, 9. middle trapezius (MTRA), 8. anterior deltoid (ADEL), 7. latissimus dorsi (LATS), 6. pectoralis major (PECC), 5. posterior deltoid (PDEL), 4. infraspinatus (INFR), 3. supraspinatus (SUPR), 2. middle deltoid (MDEL), 1. serratus anterior (SERR). For the mentioned task of sagittal pick-and-place with the mentioned sEMG recording unit, the results show that SERR and MDEL directly relate to the output of the machine learning model. This analysis should be done for different tasks and different measurement units before controlling wearable robots.

The electrode shift, which is a common challenge for daily prosthesis use [40–42], has been evaluated using different participants for estimation evaluation. In Figure 9, a participant was eliminated from the training pool, the regression accuracy was estimated, and finally, the mean regression was reported as well as the minimum and maximum regression accuracy of different participants.

Since the output data (joint angle and assistive torque) was normalized in Figure 7 and Figure 9 to show fair estimation assessment, it may seem as if the data strictly follows a specific pattern and that it is possible to predict with time series analysis. However, there are several explanations as to why the data is not following an exact pattern with constant frequency. First, although the 30 cm^2 area of the lower and upper targets were similar for all participants, the participants had different body heights and segment lengths, which required different postures to complete the task. In addition, the participants were not restricted to exact trajectory patterns. Further, the motion timing was not dictated to

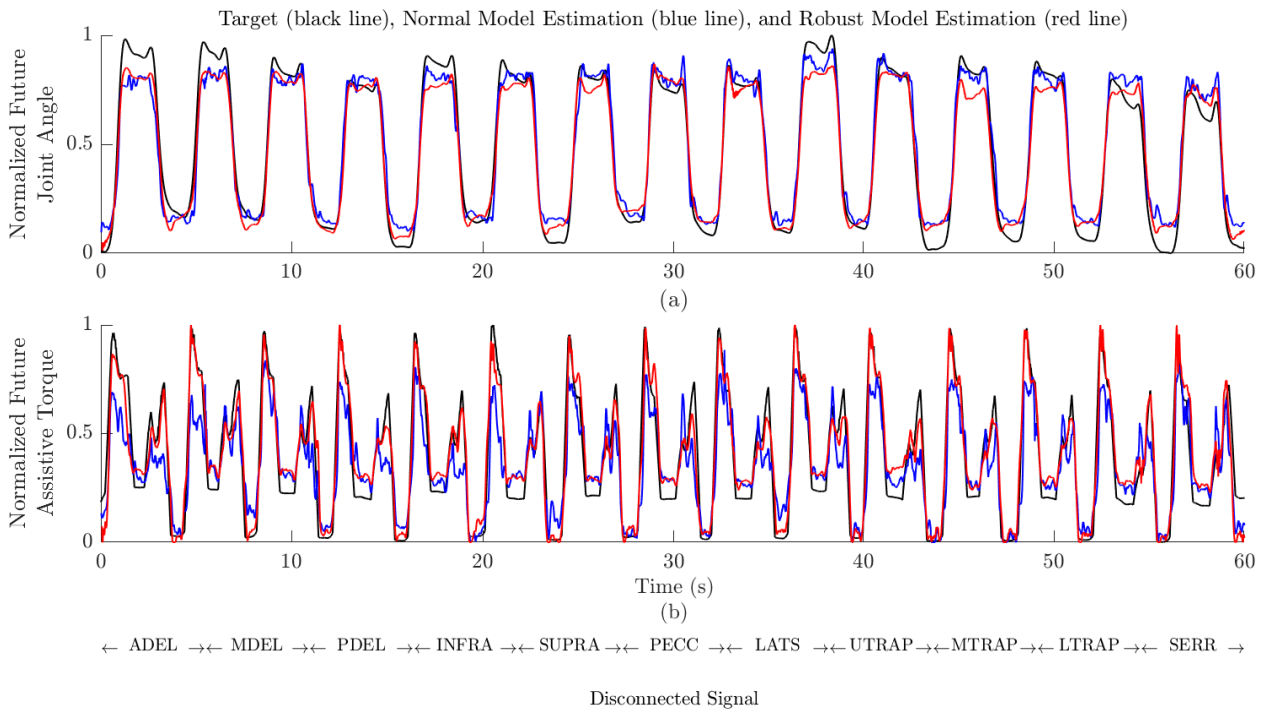

Fig. 7: Evaluation of the normal model and robust model with interrupted sEMG signals. The target output is the normalized joint angle (a) and assistive torque (b).

all participants, and participants had complete control of triggering the task.

As a further depiction of estimation ability, Figure 10 shows a section of estimation with higher resolution. The prediction horizon in Figure 10 is 0.1 seconds into the future, which means that the RNN model estimated the target that was shifted by 0.1 seconds. This RNN estimation has 0.1 seconds of shifted data compared to the synchronized mapping of biomechanical variables with sEMG signals [8]. In addition, the assistive torque is highly reliant on anthropometric data of participants, external wrench due to the object mass, and trajectory of motion. Without having information, especially the object mass, it is impossible to solve the dynamic motion Equation (5) and predict the assistive torque with time series analysis of patterns. Using the sEMG signals provides information on the activation of muscles and how the participant controls the arms according to the external object mass. For the volitional control of biomechatronic devices for non-periodic motion [7, 57], e.g., pick-and-place an object, it is practical to use sEMG signals for estimation instead of predicting using only previous kinematic data. The reasons behind this phenomenon are explained in section 1, with specific focus on the electromechanical negative delay phenomenon of sEMG signals [23] and volitional prosthesis control for amputees [40, 41].

Another point to consider regarding the RNN model application and evaluation is that this recurrent machine learning model relies highly on input and output data history. Specifically, for an RNN configuration with input signal former values (n_u) of 3 and output signal former values (n_y) of 5 (section 6.2), starting the estimation requires some previous data that is not available at $t = 0$ seconds. This study feeds the RNN model with random data at the start phase. It then continues with experimental data from when the data was available. Random input data at the beginning leads to inaccurate estimation at the beginning phase. This estimation was used as the output signal former values for further estimation. The RNN model converges in less than 2 seconds. For evaluation, a section of the estimation and target data for four participants were shown in Figure 10.

Additionally, the estimation was accomplished with the strict conditions of normalized input data (e.g., Figure 7 and Figure 9) for all participants and no sEMG information provided for the validation participant. Specifically, the maximum and minimum joint angle, velocity, acceleration, and assistive torque differed from one participant to another. The RNN model had no information on a participant's exact data (only normalized data was used) and had no information about the muscle strength and sEMG pattern of the validation par-

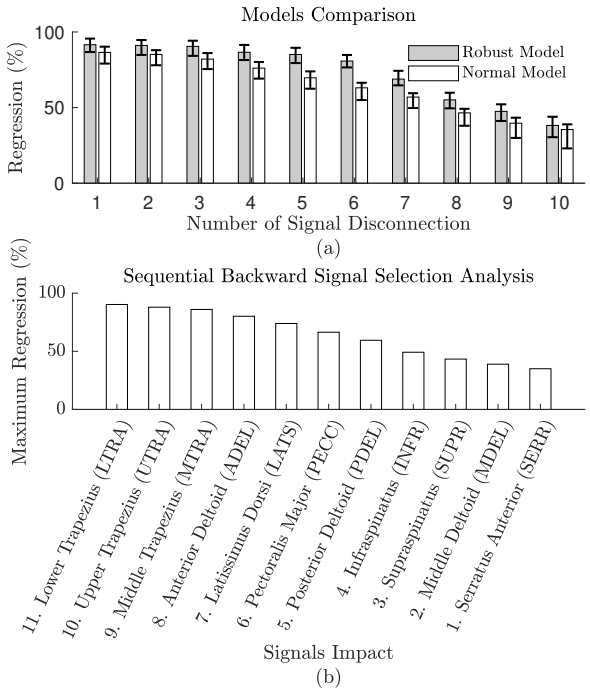

Fig. 8: Comparison of the robust and normal model with the number of interrupted sEMG signal inputs evaluated for all test participants' data (a). Signal impact versus maximum regression with sequential backward signal analysis for 11 signals (b).

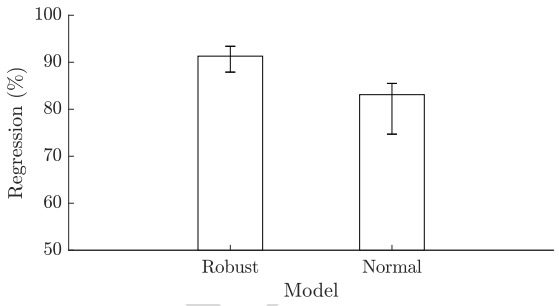

Fig. 9: Evaluation of the normal model and robust model with interrupted sEMG signals for a random participant.

ticipant, which differs from one person to the other. However, the RNN model could successfully estimate the data with regression accuracy similar to previous work [8].

6.5 Experimental evaluation

RobustMuscleNET was used for controlling the active-passive shoulder exoskeleton. Figure 11 shows the data of a participant who completed the task voluntarily. Ro-

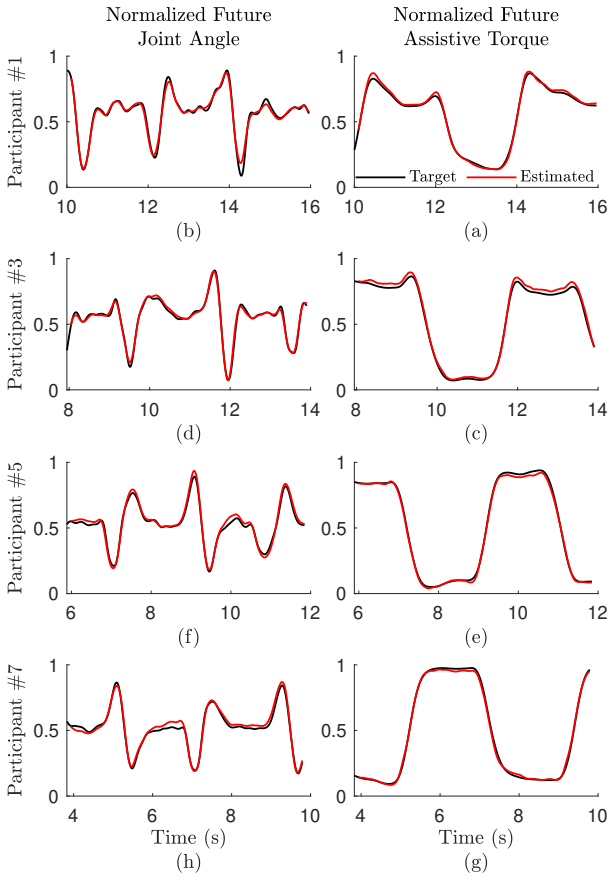

Fig. 10: A section of four participants' time-series data estimation for normalized future joint angle and assistive torque using a prediction horizon of 0.1 seconds. These participants had fairly similar anthropometric data (body height and mass) that was close to the average.

bustMuscleNET assisted in increasing the control loop speed as the human to robot variables did not require converting, resulting in an output with a 200 milliseconds prediction horizon. The prediction feature helps ensure that the systems are cooperating. Specifically, consider a scenario when the system is estimating the current joint angle and torque while the connection system has a small delay. The delayed assisting torque may oppose the desired user intention, resulting in a lack of cooperation between the robot and human. An example of this is if the user is holding a weight and wants to lower the arm while the delayed estimation system still estimates holding. The system would therefore inhibit the user from lowering their arm.

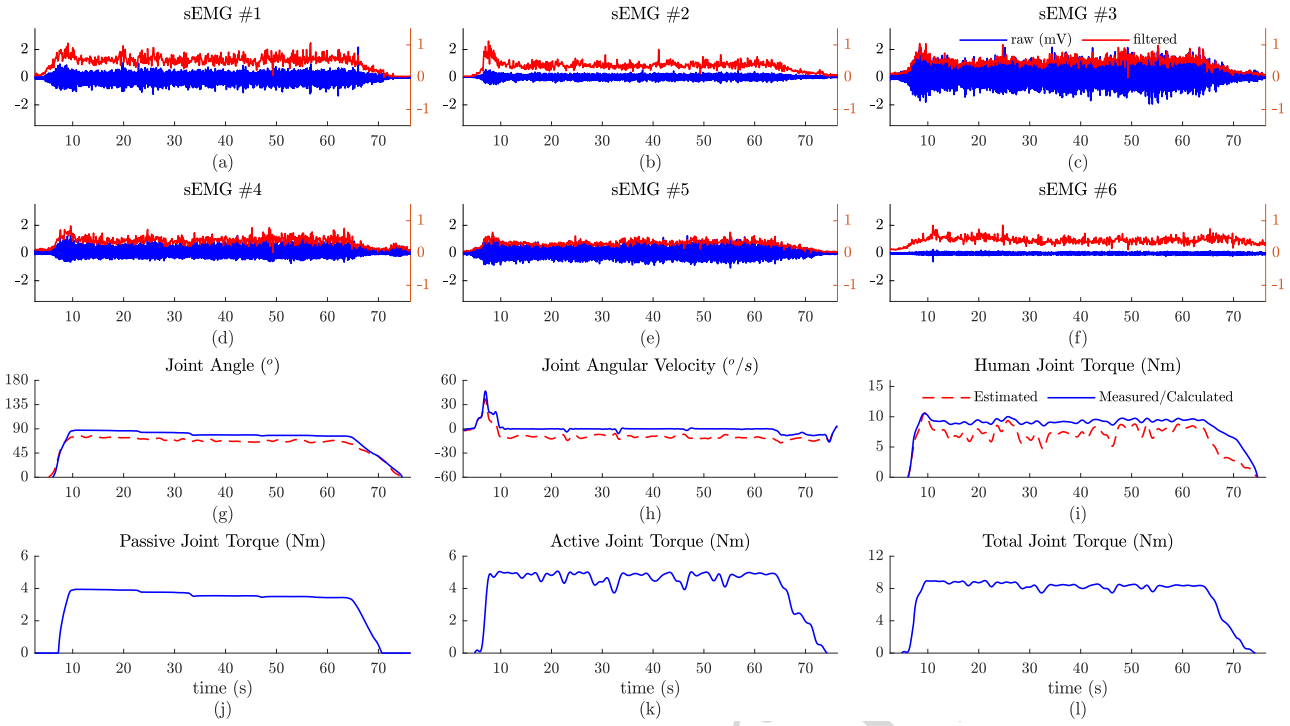

Fig. 11: (a-f) the raw and filtered sEMG signals #1-6: UTRA, MTRA, MDEL, PDEL, ADEL, and BRD; (g) the predicted exoskeleton elevation angle, (h) the predicted exoskeleton elevation angular velocity, (i) the human contribution torque estimated by RobustMuscleNET model, (j) the robot passive torque, (k) the robot feedforward torque, (l) the total robot torque.

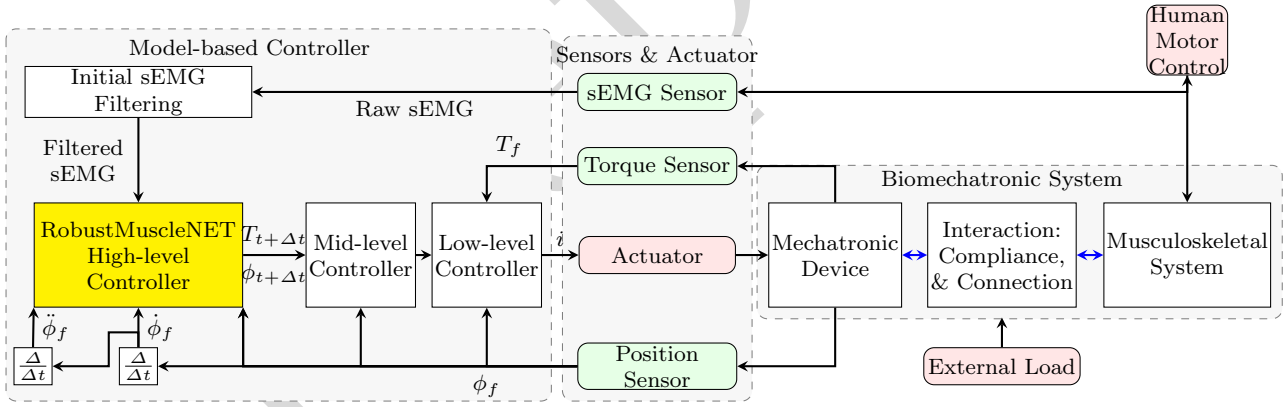

Fig. 12: The schematic for controlling an exoskeleton, prosthesis, or rehabilitation robot using RobustMuscleNET as a model for mapping the raw sEMG, joint feedback position ϕ_f, velocity $\dot{\phi}_f$, and acceleration $\ddot{\phi}_f$ to future assistive torque $\tau_{t+\Delta t}$ and future joint angle $\phi_{t+\Delta t}$. The mid and low-level controller are responsible for regulating the assistive torque and decreasing the actuator error, respectively.

6.6 Application

The robust predictive control-oriented model can be used for the high-level control of biomechatronic devices, such as exoskeletons, prostheses, and assistive / resistive robots. This high-level controller predicted the user intent based on the sEMG signal and the robot's kinematics. Since sEMG signals may disconnect in practice, the robust model supersedes a normal model in a human-in-loop control system. Since the model output was normalized to the maximum value, it is recoverable by multiplying by the maximum value. This proposed volitional myoelectric-based control loop using the robust mapping (as high-level control) is displayed in Fig-

ure 12. For the preparation of this model, offline sEMG, kinematic, and kinetic data was used.

Although this model has been evaluated for a 1-DoF exoskeleton, it can be used for multi-DoFs biomechatronic systems. In this case, the model's input should be enriched with more signals, data, and complex tasks relevant to more degrees of freedom when training the RNN.

It is noteworthy to mention that the low-level controller in Figure 12 is responsible for

1. adjusting the command according to the strength and goal of the biomechatronic devices,
2. considering the human-robot adaptation phenomenon,
3. maintaining the applied wrench according to the desired command [7, 8].

For example, a rehabilitation robot may require having a resistive torque instead of assistive torque, or a power augmentation device may require more assistive torque than the human portion [5]. This low-level controller would require further study, which is out of the scope of this paper.

For a prosthesis, since the amputated limb cannot be used for offline modeling and training of the RobustMuscleNET model, the intact mirrored limb may be used for data recording and training the model given that the use of sEMG signals from the remaining limb has been studied further [40, 41]. However, the idea of training the RobustMuscleNET model with interrupted input sEMG signals and future control-oriented output signals still contributes to prosthetics control.

7 Conclusion

A recurrent neural network developed a successful robust predictive regression-based model for mapping interrupted sEMG signals to future control-oriented signals. The output of the machine learning model implemented control-oriented biomechatronic signals instead of human biomechanical signals. This control-oriented model decreases computational cost and eliminates the optimization loop for assistive torque computation. Besides that, using future variables instead of the current variable raises the opportunity of high-level controlling the system without delay. Using an interrupted sEMG signal for model training increases the robustness of modeling in the case of disconnection and associated signal loss during online sEMG measurement. The robust predictive control-oriented regression model offers the potential to transform practical volitional myoelectric-based control of biomechatronic devices, such as exoskeletons, prostheses, and assistive / resistive robots.

In future work, training the model with random movements of varying velocities, application to prosthesis control for phantom motion intent interpretation, the repeatability of the high-level controller for electrode shift, and the low-level hierarchical control, which manages the human-robot interaction, assistance/resistance strategy weight, and coordinates the actuator, requires further study.

Acknowledgements This research is supported by funding from the Canada Research Chairs Program and the Natural Sciences and Engineering Research Council of Canada. The authors wish to thank Ekso Bionics Holdings Inc. for providing the Ekso EVO passive shoulder exoskeleton.

Author contributions Conceptualization, A.N. and J.M.; methodology, A.N.; software, A.N.; formal analysis, A.N., C.R.D., and J.M.; data acquisition, A.N. and R.L.W.; writing original draft preparation, A.N.; writing review and editing, A.N., S.B., C.R.D., and J.M.; visualization, A.N.; supervision, project administration, and funding acquisition, J.M. All authors have read and agreed to the published version of the manuscript.

Institutional review board statement The study was conducted according to the guidelines of the Declaration of Helsinki, and approved by the Office of Research Ethics of the University of Waterloo #21246 and #43980.

Data availability statement The data generated and/or analyzed during the current study are not publicly available for legal/ethical reasons but are available from the corresponding author on reasonable request.

Competing interests The authors have no competing interests that might be perceived to influence the results and/or discussion reported in this paper.

References

1. Z. Yang, S. Guo, K. Suzuki, Y. Liu, and M. Kawanishi, "An EMG-based biomimetic variable stiffness modulation strategy for bilateral motor skills relearning of upper limb elbow joint rehabilitation," *Journal of Bionic Engineering*, 2023.
2. D. Copaci, D. Serrano, L. Moreno, and D. Blanco, "A high-level control algorithm based on sEMG signalling for an elbow joint SMA exoskeleton," *Sensors*, vol. 18, no. 8, p. 2522, 2018.
3. A. J. Young and D. P. Ferris, "State of the art and future directions for lower limb robotic exoskeletons," *IEEE Transactions on Neural Systems and Rehabilitation Engineering*, vol. 25, no. 2, pp. 171–182, 2017.
4. A. Nasr, S. Bell, and J. McPhee, "Optimal design of active-passive shoulder exoskeletons: A computational modeling of human-robot interaction," *Multibody System Dynamics*, vol. 57, p. 73–106, 2023.
5. N. Li, T. Yang, Y. Yang, W. Chen, P. Yu, C. Zhang, N. Xi, Y. Zhao, and W. Wang, "Designing unpowered shoulder complex exoskeleton via contralateral drive for self-rehabilitation of post-stroke hemiparesis," *Journal of Bionic Engineering*, 2022.
6. C. Nguiadem, M. Raison, and S. Achiche, "Motion planning of upper-limb exoskeleton robots: A review," *Applied Sciences*, vol. 10, no. 21, pp. 1–21, 2020.

7. A. Nasr, B. Laschowski, and J. McPhee, "Myoelectric control of robotic leg prostheses and exoskeletons: A review," in *Proceedings of the ASME International Design Engineering Technical Conferences & Computers and Information in Engineering Conference*, vol. 85444. Online, Virtual: ASME, 2021, pp. 2021–69 203.
8. A. Nasr, S. Bell, J. He, R. L. Whittaker, N. Jiang, C. R. Dickerson, and J. McPhee, "MuscleNET: Mapping electromyography to kinematic and dynamic biomechanical variables," *Journal of Neural Engineering*, vol. 18, no. 4, p. 0460d3, 2021.
9. B. Ghannadi, R. S. Razavian, and J. McPhee, "Upper extremity rehabilitation robots: A survey," in *Handbook of Biomechatronics*. San Diego, CA, USA: Elsevier, 2018, ch. 9, pp. 319–353.
10. G. Gaudet, M. Raison, and S. Achiche, "Current trends and challenges in pediatric access to sensorless and sensor-based upper limb exoskeletons," *Sensors*, vol. 21, no. 10, 2021.
11. C. Yang, X. Xi, S. Chen, S. M. Miran, X. Hua, and Z. Luo, "SEMG-based multifeatures and predictive model for knee-joint-angle estimation," *AIP Advances*, vol. 9, no. 9, p. 095042, 2019.
12. K. Zhu, T. Xue, T. Zhang, and M. Zhang, "SEMG-based joint moment estimation for hip exoskeleton general assistive strategy," in *Proceedings of the Chinese Automation Congress*. Hangzhou, China: IEEE, 2019, pp. 3826–3830.
13. J. Wang, D. Wu, Y. Gao, X. Wang, X. Li, G. Xu, and W. Dong, "Integral Real-time Locomotion Mode Recognition Based on GA-CNN for Lower Limb Exoskeleton," *Journal of Bionic Engineering*, vol. 19, no. 5, pp. 1359–1373, 2022.
14. T. Yao, J. Lv, L. Yang, A. Xu, and S. Qu, "Design of the pneumatic pressure smart shoes for an ankle-assisted exoskeleton," *Journal of Bionic Engineering*, 2023.
15. A. Rudenko, L. Palmieri, M. Herman, K. M. Kitani, D. M. Gavrila, and K. O. Arras, "Human motion trajectory prediction: A survey," *International Journal of Robotics Research*, vol. 39, no. 8, pp. 895–935, 2020.
16. K. Abdel-Malek and J. Arora, *Human motion simulation: Predictive dynamics*. Elsevier, 2013.
17. M. Asghari Oskoei and H. Hu, "Myoelectric control systems-A survey," *Biomedical Signal Processing and Control*, vol. 2, no. 4, pp. 275–294, 2007.
18. M. Akmal, S. Zubair, M. Jochumsen, E. N. Kamavuako, and I. K. Niazi, "A tensor-based method for completion of missing electromyography data," *IEEE Access*, vol. 7, pp. 104 710–104 720, 2019.
19. A. Naber, E. Mastinu, and M. Ortiz-Catalan, "Stationary wavelet processing and data imputing in myoelectric pattern recognition on a low-cost embedded system," *IEEE Transactions on Medical Robotics and Bionics*, vol. 1, no. 4, pp. 256–266, 2019.
20. R. M. Singh, S. Chatterji, and A. Kumar, "A review on surface EMG based control schemes of exoskeleton robot in stroke rehabilitation," in *Proceedings of the International Conference on Machine Intelligence Research and Advancement*, IEEE. Katra, India: IEEE, 2014, pp. 310–315.
21. G. Durandau, D. Farina, and M. Sartori, "Robust real-time musculoskeletal modeling driven by electromyograms," *IEEE Transactions on Biomedical Engineering*, vol. 65, no. 3, pp. 556–564, 2018.
22. Y. Liu, D. Xin, J. Hua, and M. Liu, "SEMG motion intention recognition based on wavelet time-frequency spectrum and ConvLSTM," *Journal of Physics: Conference Series*, vol. 1631, no. 1, 2020.
23. S. Conforto, P. A. Mathieu, M. Schmid, D. Bibbo, J. R. Florestal, and T. D'Alessio, "How much can we trust the electromechanical delay estimated by using electromyography?" in *Proceedings of the Annual International Conference of the IEEE Engineering in Medicine and Biology*. New York, NY, USA: IEEE, 2006, pp. 1256–1259.
24. H. Sözen, E. Cè, A. V. Bisconti, S. Rampichini, S. Longo, G. Coratella, S. Shokohyar, C. Doria, M. Borrelli, E. Limonta, and F. Esposito, "Differences in electromechanical delay components induced by sex, age and physical activity level: New insights from a combined electromyographic, mechanomyographic and force approach," *Sport Sciences for Health*, vol. 15, no. 3, pp. 623–633, 2019.
25. G. Durandau, D. Farina, G. Asín-Prieto, I. Dimbwadyo-Terrer, S. Lerma-Lara, J. L. Pons, J. C. Moreno, and M. Sartori, "Voluntary control of wearable robotic exoskeletons by patients with paresis via neuromechanical modeling," *Journal of NeuroEngineering and Rehabilitation*, vol. 16, no. 1, pp. 1–18, 2019.
26. A. Nasr, S. Ferguson, and J. McPhee, "Model-based design and optimization of passive shoulder exoskeletons," in *Proceedings of the ASME International Design Engineering Technical Conferences & Computers and Information in Engineering Conference*. Online, Virtual: ASME, 2021, pp. 2021–69 437.
27. R. Gopura, K. Kiguchi, and Y. Yi, "SUEFUL-7: A 7DOF upper-limb exoskeleton robot with muscle-model-oriented EMG-based control," in *Proceedings of the IEEE/RSJ International Conference on Intelligent Robots and Systems*. St. Louis, MO, USA: IEEE, 2009, pp. 1126–1131.
28. P. Malcolm, S. Galle, and D. De Clercq, "Fast exoskeleton optimization," *Science*, vol. 356, no. 6344, pp. 1230–1231, 2017.
29. Y. Hayashi, R. Dubey, and K. Kiguchi, "Torque optimization for a 7DOF upper-limb power-assist exoskeleton robot," in *Proceedings of the IEEE Workshop on Robotic Intelligence In Informationally Structured Space*. Paris, France: IEEE, 2011, pp. 49–54.
30. M. Sarac, M. Solazzi, E. Sotgiu, M. Bergamasco, and A. Frisoli, "Design and kinematic optimization of a novel underactuated robotic hand exoskeleton," *Meccanica*, vol. 52, no. 3, pp. 749–761, 2017.
31. L. Zhou, Y. Li, and S. Bai, "A human-centered design optimization approach for robotic exoskeletons through biomechanical simulation," *Robotics and Autonomous Systems*, vol. 91, pp. 337–347, 2017.
32. J. Zhang, P. Fiers, K. A. Witte, R. W. Jackson, K. L. Poggensee, C. G. Atkeson, and S. H. Collins, "Human-in-the-loop optimization of exoskeleton assistance during walking," *Science*, vol. 356, no. 6344, pp. 1280–1283, 2017.
33. A. Hashemi and J. McPhee, "Assistive sliding mode control of a rehabilitation robot with automatic weight adjustment," in *Proceedings of the 43rd Annual International Conference of the IEEE Engineering in Medicine & Biology Society*. Mexico: IEEE, 2021, pp. 4891–4896.
34. N. Mehrabi, R. S. Razavian, B. Ghannadi, and J. McPhee, "Predictive simulation of reaching moving targets using nonlinear model predictive control," *Frontiers in Computational Neuroscience*, vol. 10, p. 143, 2017.
35. C. Chen, K. Huang, D. Li, Z. Zhao, and J. Hong, "Multi-segmentation parallel CNN model for estimating assem-

bly torque using surface electromyography signals," *Sensors*, vol. 20, no. 15, pp. 1–22, 2020.
36. C. Li, G. Li, G. Jiang, D. Chen, and H. Liu, "Surface EMG data aggregation processing for intelligent prosthetic action recognition," *Neural Computing and Applications*, vol. 32, no. 22, pp. 16 795–16 806, 2020.
37. J. Liu, S. H. Kang, D. Xu, Y. Ren, S. J. Lee, and L. Q. Zhang, "EMG-Based continuous and simultaneous estimation of arm kinematics in able-bodied individuals and stroke survivors," *Frontiers in Neuroscience*, vol. 11, p. 480, 2017.
38. Y. Zhang, X. Zhang, Z. Lu, Z. Jiang, and T. Zhang, "A novel wrist joint torque prediction method based on EMG and LSTM," in *Proceedings of the 10th IEEE International Conference on Cyber Technology in Automation, Control and Intelligent Systems*. Xi'an, China: IEEE, 2020, pp. 242–245.
39. A. Fleming, N. Stafford, S. Huang, X. Hu, D. P. Ferris, and H. H. Huang, "Myoelectric control of robotic lower limb prostheses: A review of electromyography interfaces, control paradigms, challenges and future directions," *Journal of Neural Engineering*, vol. 18, p. 041004, 2021.
40. A. Fougner, O. Stavdahl, P. J. Kyberd, Y. G. Losier, and P. A. Parker, "Control of upper limb prostheses: Terminology and proportional myoelectric controla review," *IEEE Transactions on Neural Systems and Rehabilitation Engineering*, vol. 20, no. 5, pp. 663–677, 2012.
41. E. Nsugbe, O. W. Samuel, M. G. Asogbon, and G. Li, "Phantom motion intent decoding for transhumeral prosthesis control with fused neuromuscular and brain wave signals," *IET Cyber-Systems and Robotics*, vol. 3, no. 1, pp. 77–88, 2021.
42. L. M. Vaca Benitez, M. Tabie, N. Will, S. Schmidt, M. Jordan, and E. A. Kirchner, "Exoskeleton technology in rehabilitation: Towards an EMG-based orthosis system for upper limb neuromotor rehabilitation," *Journal of Robotics*, vol. 2013, p. 610589, 2013.
43. R. L. Whittaker, W. Park, and C. R. Dickerson, "Application of a symbolic motion structure representation algorithm to identify upper extremity kinematic changes during a repetitive task," *Journal of Biomechanics*, vol. 72, pp. 235–240, 2018.
44. B. T. Kelly, W. R. Kadrmas, and K. P. Speer, "The manual muscle examination for rotator cuff strength: An electromyographic investigation," *American Journal of Sports Medicine*, vol. 24, no. 5, pp. 581–588, 1996.
45. G. D. Pope, "Introduction to surface electromyography," *Physiotherapy*, vol. 84, no. 8, p. 405, 1998.
46. R. L. Whittaker, N. J. La Delfa, and C. R. Dickerson, "Algorithmically detectable directional changes in upper extremity motion indicate substantial myoelectric shoulder muscle fatigue during a repetitive manual task," *Ergonomics*, vol. 62, no. 3, pp. 431–443, 2019.
47. S. Galle, P. Malcolm, W. Derave, and D. De Clercq, "Adaptation to walking with an exoskeleton that assists ankle extension," *Gait and Posture*, vol. 38, no. 3, pp. 495–499, 2013.
48. A. Nasr, A. Hashemi, and J. McPhee, "Model-based mid-level regulation for assist-as-needed hierarchical control of wearable robots: A computational study of human-robot adaptation," *Robotics*, vol. 11, no. 1, p. 20, 2022.
49. N. Mehrabi, M. S. Shourijeh, and J. McPhee, "Study of human steering tasks using neuromuscular driver model," in *International Symposium on Advanced Vehicle Control*, Seoul, Korea, 2012, pp. 1–6.
50. A. Nasr and J. McPhee, "Biarticular MuscleNET: A machine learning model of biarticular muscles," in *Proceedings of the North American Congress on Biomechanics*, Ottawa, Canada, 2022.
51. ——, "Multibody constrained dynamic modelling of human-exoskeleton: Toward optimal design and control of an active-passive wearable robot," in *Proceedings of the 6th Joint International Conference on Multibody System Dynamics and the 10th Asian Conference on Multibody System Dynamics*. New Dehli, India: Springer, 2022, p. 189.
52. K. A. Inkol, C. Brown, W. McNally, C. Jansen, and J. McPhee, "Muscle torque generators in multibody dynamic simulations of optimal sports performance," *Multibody System Dynamics*, vol. 50, no. 4, pp. 435–452, 2020.
53. G. Wu, F. C. Van Der Helm, H. E. Veeger, M. Makhsous, P. Van Roy, C. Anglin, J. Nagels, A. R. Karduna, K. McQuade, X. Wang, F. W. Werner, and B. Buchholz, "ISB recommendation on definitions of joint coordinate systems of various joints for the reporting of human joint motion - Part II: Shoulder, elbow, wrist and hand," *Journal of Biomechanics*, vol. 38, no. 5, pp. 981–992, 2005.
54. A. Nasr, S. Ferguson, and J. McPhee, "Model-based design and optimization of passive shoulder exoskeletons," *Journal of Computational and Nonlinear Dynamics*, vol. 17, no. 5, p. 051004, 2022.
55. C. J. De Luca, L. Donald Gilmore, M. Kuznetsov, and S. H. Roy, "Filtering the surface EMG signal: Movement artifact and baseline noise contamination," *Journal of Biomechanics*, vol. 43, no. 8, pp. 1573–1579, 2010.
56. M. B. I. Reaz, S. Hussain, and F. Mohd-Yasin, "Techniques of EMG signal analysis: Detection, processing, classification and applications," *Biological procedures online*, vol. 8, no. 1, pp. 11–35, 2006.
57. O. A. Kannape and H. M. Herr, "Volitional control of ankle plantar flexion in a powered transtibial prosthesis during stair-ambulation," in *Proceedings of the 36th Annual International Conference of the IEEE Engineering in Medicine and Biology Society*. Chicago, IL, USA: IEEE, 2014, pp. 1662–1665.
58. M. S. Shourijeh, R. S. Razavian, and J. McPhee, "Estimation of maximum finger tapping frequency using musculoskeletal dynamic simulations," *Journal of Computational and Nonlinear Dynamics*, vol. 12, no. 5, p. 051009, 2017.
59. A. Nasr, J. He, N. Jiang, and J. McPhee, "Muscle modelling using machine learning and optimal filtering of sEMG signals," in *Proceedings of the 45th Meeting of the American Society of Biomechanics*, Virtual, 2021, p. 83.
60. R. S. Razavian, B. Ghannadi, and J. McPhee, "On the relationship between muscle synergies and redundant degrees of freedom in musculoskeletal systems," *Frontiers in Computational Neuroscience*, vol. 13, p. 23, 2019.